

Quantitative analysis of an anaphase B switch: predicted role for a microtubule catastrophe gradient

Dhanya K. Cheerambathur,¹ Gul Civelekoglu-Scholey,^{1,2} Ingrid Brust-Mascher,¹ Patrizia Sommi,¹ Alex Mogilner,² and Jonathan M. Scholey¹

¹Department of Molecular and Cellular Biology and ²Department of Neurobiology, Physiology, and Behavior, University of California at Davis, Davis, CA 95616

Anaphase B in *Drosophila* embryos is initiated by the inhibition of microtubule (MT) depolymerization at spindle poles, which allows outwardly sliding interpolar (ip) MTs to drive pole–pole separation. Using fluorescence recovery after photobleaching, we observed that MTs throughout the preanaphase B spindle are very dynamic and display complete recovery of fluorescence, but during anaphase B, MTs proximal to the poles stabilize and therefore display lower recovery than those elsewhere. Fluorescence microscopy of the MT tip tracker EB1 revealed that growing MT plus ends localize

throughout the preanaphase B spindle but concentrate in the overlap region of interpolar MTs (ipMTs) at anaphase B onset. None of these changes occurred in the presence of nondegradable cyclin B. Modeling suggests that they depend on the establishment of a spatial gradient of MT plus-end catastrophe frequencies, decreasing toward the equator. The resulting redistribution of ipMT plus ends to the overlap zone, together with the suppression of minus-end depolymerization at the poles, could constitute a mechanical switch that initiates spindle elongation.

Introduction

Chromosome segregation during mitosis depends on the action of the spindle, a protein machine that uses ensembles of kinesin and dynein motors plus microtubule (MT) dynamics to move chromatids polewards (anaphase A) and to elongate the spindle (anaphase B; Scholey et al., 2003; Gadde and Heald, 2004; Wadsworth and Khodjakov, 2004). Spindle MTs display “poleward flux,” a form of MT dynamics in which tubulin subunits within the MT polymer lattice translocate persistently poleward while their minus ends are depolymerized at the poles (Mitchison and Salmon, 1992). In addition, prometaphase spindle MTs use dynamic instability to search for chromosomes and then capture and align them on the spindle equator (Mitchison and Kirschner, 1984; Wollman et al., 2005). However, in many spindles, MTs suddenly become stable at the onset of anaphase (Zhai et al., 1995; Mallavarapu et al., 1999; Maddox et al., 2000; Higuchi and Uhlmann, 2005). In budding yeast, the suppression of MT dynamics is regulated by the cell cycle–regulated Cdc14 phosphatase and is essential for proper chromosome segregation, as

loss of MT stabilization at anaphase onset leads to defects in both anaphase A and B (Higuchi and Uhlmann, 2005).

In the *Drosophila* syncytial blastoderm stage embryo, highly dynamic MTs drive remarkably rapid movements of chromosomes and spindle poles, at rates typically of $\sim 0.1 \mu\text{m s}^{-1}$ (Brust-Mascher and Scholey, 2002; Brust-Mascher et al., 2004; Rogers et al., 2004; Civelekoglu-Scholey et al., 2006). In preanaphase B (metaphase and anaphase A) spindles, it is proposed that a kinesin-5 (KLP61F)–driven interpolar MT (ipMT) sliding filament mechanism is balanced by kinesin-13 (KLP10A)–dependent ipMT depolymerization at the poles to maintain the spindle at a steady-state length while simultaneously driving poleward flux within ipMTs. Once chromatid-to-pole motion is essentially complete, anaphase B is triggered by the suppression of kinesin-13–dependent depolymerization, which allows persistently sliding ipMTs to exert forces that drive spindle pole separation (Brust-Mascher and Scholey, 2002; Brust-Mascher et al., 2004; Rogers et al., 2004). Here, therefore, one function of poleward flux is to constrain the length of preanaphase B spindles, and its down-regulation permits spindle elongation.

Surprisingly, the ipMTs that drive anaphase spindle elongation in *Drosophila* embryos are highly dynamic, displaying a

Correspondence to Jonathan M. Scholey: jmscholey@ucdavis.edu

Abbreviations used in this paper: ipMT, interpolar MT; kMT, kinetochore MT; MT, microtubule.

The online version of this article contains supplemental material.

turnover half-time of ~ 5 s in FRAP experiments (Brust-Mascher et al., 2004). Quantitative modeling using systems of force balance and rate equations suggests that this rapid rate of MT turnover is due to the dynamic instability of ipMT plus ends and demonstrates that such dynamic ipMTs are capable of driving steady, linear pole–pole separation at ~ 0.1 $\mu\text{m/s}$ (Brust-Mascher et al., 2004). However, it is not known if the rapid dynamics is a property of MTs at all stages of mitosis in *Drosophila* and if these spindle MTs, like those of other systems, undergo stabilization at anaphase B onset.

Here, we have systematically evaluated the dynamic properties of spindle MTs throughout mitosis in *Drosophila* embryos using FRAP of fluorescent GFP-tubulin in conjunction with time-lapse fluorescence microscopy of EB1-GFP to mark the growing MT plus ends (Rogers et al., 2002; Brust-Mascher et al., 2004). Our studies show that before anaphase B, spindle MTs turn over rapidly and display a uniform plus-end distribution, but at anaphase B onset, in a process that requires cyclin B degradation, a stable subset of MTs develops as MT plus ends specifically redistribute into the central spindle region at the expense of MTs that depolymerize near the poles. We used quantitative modeling to investigate (1) the dynamic parameters that could account for the full and rapid turnover of MT plus ends that are uniformly distributed throughout the preanaphase B spindle and (2) the changes in dynamics that could produce the spatial reorganization of MTs that occurs at anaphase B onset. The results illuminate a mechanism by which a spatial change in spindle MT dynamics may redistribute MT plus ends to facilitate anaphase B spindle elongation.

Results

***Drosophila* mitotic spindles turn over at a rapid rate during metaphase**
Using FRAP analysis of GFP-tubulin, we find that *Drosophila* embryo mitotic spindles turn over at an extremely rapid rate (half-time of 5–10 s) and recover almost completely during preanaphase B (i.e., the metaphase–anaphase A steady state; Fig. 1, Fig. 2 A, Fig. S1 A; and Videos 1 and 2, available at <http://www.jcb.org/cgi/content/full/jcb.200611113/DC1>) in accordance with our previous analysis of the equatorial region of anaphase B spindles (Brust-Mascher et al., 2004). These preanaphase B spindle MTs could plausibly turn over by dynamic instability of their plus ends and/or by poleward flux (Salmon et al., 1984; Saxton et al., 1984; Wadsworth and Salmon, 1986; Mallavarapu et al., 1999; Zhai et al., 1995). The rate of poleward flux in these spindles (0.05 $\mu\text{m/s}$) on its own is too slow to account for the fast FRAP recovery, especially within the large bleach regions of preanaphase B spindles (see the supplemental text), so the rapid turnover is most likely due to MT dynamic instability superimposed on poleward flux (Brust-Mascher et al., 2004).

Several controls suggest that our FRAP experiments are faithfully reporting spindle MT polymer dynamics; for example, spindle MTs do not turn over in the presence of the drug taxol, which inhibits MT polymer dynamics (Fig. S1 B). The fast recovery is unlikely to be due solely to the diffusion of

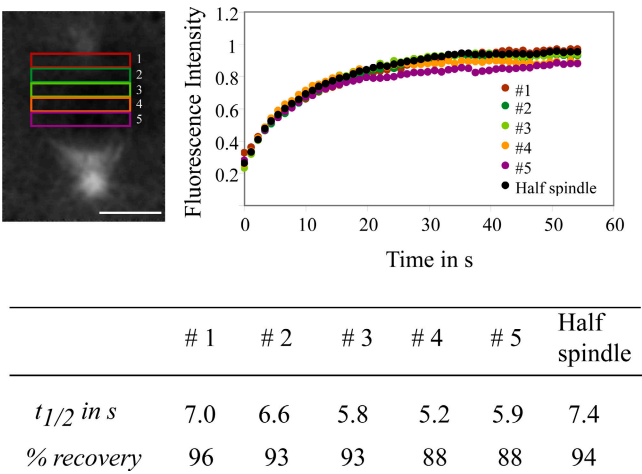


Figure 1. MTs turn over rapidly in a preanaphase B spindle, and the fluorescence recovery is uniform within a bleached region. The micrograph shows a spindle in preanaphase B, bleached in a 5- μm -wide region extending from the centrosome to the equator (half-spindle). The 5- μm bleached region was divided into 1- μm subsegments to analyze the recovery kinetics along the length of the spindle axis. The plots on the right are the recovery curves of the half-spindle and individual 1- μm subsegments, and the table below shows their half-time and percentage of recovery. Note that there is no notable difference in half-time or percentage of recovery of the half-spindle and the 1- μm subsegments. See also Video 1 (available at <http://www.jcb.org/cgi/content/full/jcb.200611113/DC1>). Bar, 5 μm .

unassembled GFP-tubulin subunits, because in 5- μm -wide bleach regions outside the spindle, in which tubulin dynamics is governed by subunit diffusion, the recovery half-time is < 1 s, much faster than that observed in spindles (unpublished data).

Importantly, the turnover is independent of both the size of the bleached zone and its position along the long axis of the metaphase spindle. For example, the kinetics and extent of fluorescence recovery were very similar within several adjacent 1- μm -wide subregions of a larger, 5- μm bleach region ($t_{1/2} = 7.4$ s; percentage recovery $\sim 94\%$), indicating that FRAP was uniform throughout the bleached area (Fig. 1 and Video 1). The observation suggests that the recovery could result from the exchange of tubulin subunits all along the pole–pole axis of the spindle. Interestingly, if we assume that tubulin subunits exchange only at the plus and minus ends and not at internal sites within the MT polymer lattice, these results are consistent with the view that dynamic MT ends are present throughout the spindle (see section Model Result 1).

A spatially regulated change in MT dynamics at anaphase B onset
Spindle MTs are stabilized at anaphase onset in yeast and vertebrate cells (Zhai et al., 1995; Mallavarapu et al., 1999; Maddox et al., 2000; Higuchi and Uhlmann, 2005), so to see if a similar change in MT dynamics occurs within *Drosophila* embryo spindles, we monitored FRAP recovery before and after anaphase B onset (Fig. 2). These spindles characteristically remain in the preanaphase B steady state for ~ 100 s before elongating during anaphase B (from ~ 10 – 12 to ~ 14 – 16 μm), so we used pole–pole separation as a visual cue to detect the onset of anaphase B in FRAP experiments. Our studies showed that the

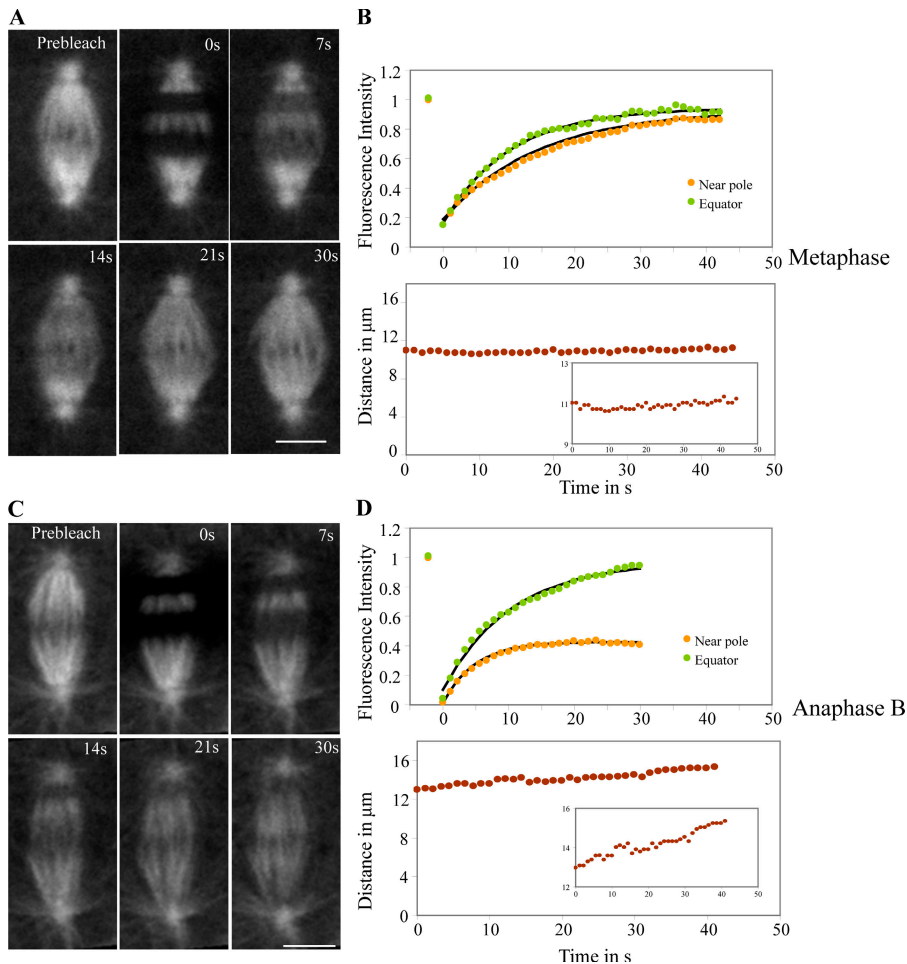


Figure 2. Anaphase B spindles exhibit a spatial difference in MT turnover compared with preanaphase B spindles. (A) Micrographs of a preanaphase B spindle bleached simultaneously at two separate regions. See also Video 2 (available at <http://www.jcb.org/cgi/content/full/jcb.200611113/DC1>). (B) Normalized fluorescence recovery curves of the two bleach zones and exponential fits (black lines). During preanaphase B, both regions recover to the same extent, $\sim 85\%$ with $t_{1/2}$ of 8 and 5 s at the pole and equator, respectively. In the bottom panel, constant pole–pole distance shows that the spindle is in preanaphase B steady state. (C) Micrographs of an anaphase B spindle bleached simultaneously near the pole and equator. See also Video 3. (D) The normalized fluorescence recovery curves of the two bleach zones with their corresponding exponential fits (black lines). The bleached zone closer to the pole recovers to a strikingly lower extent, $\sim 40\%$ compared with that in the spindle equator, $\sim 90\%$, and $t_{1/2}$ is 3 and 5 s at the pole and equator, respectively. The bottom panel shows an increasing pole–pole distance, indicating that the spindle is in anaphase B. The insets in the graphs in B and D show higher resolution plots of pole–pole distance versus time. Bars, 5 μm .

half-time of recovery was the same before and after anaphase B onset, but there was a notable, position-dependent difference in the percentage of recovery during anaphase B spindle elongation (Fig. 2, C and D; Video 3, available at <http://www.jcb.org/cgi/content/full/jcb.200611113/DC1>; and Table I). Regions proximal to the spindle equator displayed similar fluorescence recovery to preanaphase B spindles ($t_{1/2}$ of 5 s and 86% recovery), but in regions proximal to the poles, the extent of recovery was substantially reduced (to $\sim 46\%$ with a $t_{1/2}$ of 2.8 s). These differences in recovery are consistent with a spatially regulated change in MT dynamics at anaphase B onset, which results in the evolution of two populations of MTs near the poles; a small dynamic subset of MTs that continue to turn over rapidly and recover their fluorescence, and a second, new, stable subset of MTs that do not undergo detectable turnover, accounting for the lower extent of fluorescence recovery.

MT plus ends display a uniform distribution in preanaphase B spindles and redistribute to the central spindle at anaphase B onset

If the turnover primarily reflects dynamic instability of MT plus ends, the aforementioned spatial change in MT polymer dynamics at anaphase B onset should correspond to an alteration in the spatial distribution of MT plus ends. To test this idea, we monitored the dynamics of EB1 (a “plus-end tip tracker,” which

localizes to growing MT plus ends) using time-lapse imaging of transgenic fly embryos expressing an EB1 fusion protein containing GFP at its C terminus (Rogers et al., 2002; Piehl and Cassimeris, 2003). Mitosis progressed normally in these embryos, suggesting that EB1-GFP expression did not create any obvious defects. The EB1-GFP formed comets that displayed antipoleward motility at $0.25 \pm 0.2 \mu\text{m/s}$ (not depicted) and underwent a stage-specific relocalization; the comets were distributed uniformly throughout preanaphase B spindles, but at anaphase B onset, they redistributed into a 3–4- μm -wide band at the spindle equator (Fig. 3, A and B; and Video 4, available at <http://www.jcb.org/cgi/content/full/jcb.200611113/DC1>). Assuming that EB1 specifically marks the plus ends of growing MTs, as expected, then this redistribution must reflect changes in the distribution of growing MT plus ends, which would support our hypothesis that the spatial changes in MT turnover measured in the FRAP analysis of spindles before and after anaphase B onset reflects a change in MT plus-end distribution. We infer that MT plus ends, located throughout the half spindles, redistribute to the spindle midzone and, furthermore, by using kymography to track EB1-GFP throughout the whole spindle, we determined that this redistribution occurs abruptly at anaphase B onset when the spindle starts to elongate (Fig. 3 D; Fig. S2 B; and Video 4). Thus, at anaphase B onset, there is a change in MT dynamics that leads to the rapid redistribution of MT plus ends

Table I. MT turnover during metaphase and preanaphase B in wild-type and stable GST–cyclin B–injected spindles in *Drosophila* embryos

Embryo	Mitotic stage	Near pole		Equator	
		$t_{1/2}$	Percentage of recovery	$t_{1/2}$	Percentage of recovery
		s		s	
Wild type	Preanaphase B	8.6 ± 2.3 ($n = 10$)	81.0 ± 14.3 ($n = 10$)	5.8 ± 0.9 ($n = 11$)	89.5 ± 6.8 ($n = 11$)
Wild type	Anaphase B	2.8 ± 0.5 ($n = 20$)	45.8 ± 11.2 ($n = 20$)	5.3 ± 1.3 ($n = 20$)	85.8 ± 8.8 ($n = 20$)
Stable cyclin B injected	Preanaphase B arrested	7.8 ± 2.2 ($n = 23$)	85.0 ± 8.13 ($n = 23$)	6.57 ± 0.9 ($n = 20$)	88.0 ± 8.6 ($n = 20$)

The $t_{1/2}$ and percentage of recovery values for the pole and equator shown in the table are from experiments where the spindles were simultaneously bleached at the two regions.

from throughout the half-spindles to the spindle midzone, where the overlapping plus ends of antiparallel ipMTs are found.

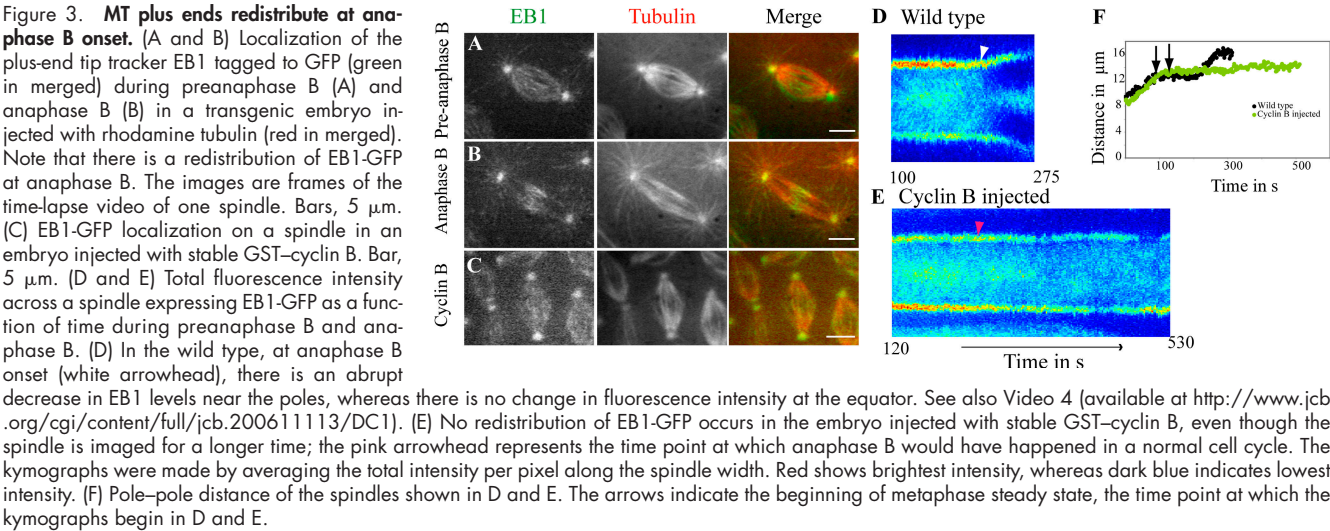
The spatial change in MT dynamics at anaphase B onset requires cyclin B degradation

To test the role of cyclin B degradation, which is required for cell cycle progression from metaphase through mitotic exit (Wheatley et al., 1997; Pines, 2006), we injected a stable, nondegradable *Drosophila* GST–cyclin B fusion protein into embryos expressing GFP–tubulin or GFP–histone (Su et al., 1998; Royou et al., 2002). The injected embryos displayed a gradient of phenotypes, with spindles proximal to the injection site arresting in metaphase and not exiting for at least 15 min (Fig. S2 A). Spindles further away from the injection site progressed slowly through anaphase A and partially or completely segregated their chromatids after a slight delay (Fig. 4 A). These spindles, which we term anaphase A–arrested, never entered anaphase B but instead maintained constant pole–pole spacing. The metaphase- and anaphase A–arrested spindles displayed MT turnover similar to that of wild-type preanaphase B spindles in FRAP experiments with nearly complete recoveries both proximal to the poles and at the equator (Fig. 4 B and Table I). In addition, fluorescence speckle microscopy showed persistent poleward flux, suggesting that the depolymerase KLP10A at the poles remained active (Brust-Mascher et al., 2004; unpublished data). Finally, these arrested spindles maintained a persistent, uniform distribution of

EB1-GFP (Fig. 3, C and E), even after anaphase A chromosome movement (Fig. S2 C). These observations strongly suggest that the redistribution of plus ends, the spatial change in MT dynamics, and the inactivation of the depolymerase at the poles, which occur at anaphase B onset in wild-type embryos, are initiated by a switch that requires cyclin B degradation and is therefore likely to be cell cycle regulated.

Modeling suggests a plausible mechanism underlying the redistribution of MT plus ends to the spindle midzone at anaphase B onset

The results so far suggest that cyclin B degradation initiates a signal transduction pathway that triggers the redistribution of MT plus ends to the overlap region at the spindle equator, raising questions about the molecular identity of the targets of the signal and the mechanism of redistribution. These issues are difficult to address experimentally because the perturbation of candidate target molecules such as EB1, KLP10A, KLP3A, and RanGTP can have multiple effects on spindle assembly, chromosome motility, and anaphase B (Rogers et al., 2002; Brust-Mascher et al., 2004; Kwon et al., 2004; Kalab et al., 2006; Silverman-Gavrila and Wilde, 2006), which can obscure specific effects on MT plus-end dynamics at anaphase B onset. We did observe that EB1 still redistributed to the spindle interzone in the fraction of Ran- or KLP3A-inhibited spindles that underwent partial anaphase B (Fig. S2 D), but whether a reduced



redistribution correlated with the decrease in spindle elongation was impossible to quantify.

Another problem was that the uniform distribution of MT plus ends and the rapid, full and uniform FRAP recovery observed in preanaphase B spindles could easily be explained if dynamic MT minus ends are also uniformly distributed throughout the spindle (Burbank et al., 2006; Mahoney et al., 2006; Fig. S3 B, available at <http://www.jcb.org/cgi/content/full/jcb.200611113/DC1>). However, the *Drosophila* embryo spindle assembles primarily by the centrosomal pathway, so most of its MT minus ends are likely to be proximal to the poles (McIntosh et al., 1975, 1979; Sharp et al., 1999). Such a biased distribution of minus ends, superimposed on a uniform distribution of MT plus ends, would intuitively predict a slower or less extensive recovery of a bleach mark near the pole versus the equator of preanaphase (as well as anaphase B) spindles, in contrast to what we observe (Fig. 2).

In light of these difficulties, we turned to computational modeling to elucidate (1) the MT dynamic properties and MT end distributions that could account for the rapid and nearly complete turnover of MTs during preanaphase B and (2) the mechanisms that could produce the abrupt rearrangement of MT plus ends observed at anaphase B onset to promote spindle elongation (see the supplemental text for the description of the model).

Model result 1: rapid MT turnover can be explained if MT dynamic instability parameters are fine-tuned

In our simulations, we consider hundreds of MTs asynchronously undergoing dynamic instability at their plus ends and simultaneously sliding toward the spindle poles via forces generated by the bipolar motors at the antiparallel overlaps (Brust-Mascher et al., 2004). During preanaphase B, the minus ends of “virtual” MTs depolymerize at the poles with a mean rate equal to the free sliding rate of the bipolar motors at the midzone, and because the motors work near their load-free regime, the spindle length remains constant. At the onset of anaphase B, we numerically “switch off” MT depolymerization so that MT sliding is converted into spindle elongation. In the model, the dynamics of MT plus ends is determined by the four parameters of dynamic instability: the growth and shortening rates, v_g and v_s , and the rescue and catastrophe frequencies, f_{res} and f_{cat} . Assuming that all spindle MTs obey the same dynamics (constant rates), our goal was to explore which regions of this four-dimensional parameter space, and which distributions of MT plus and minus ends could account for the observed rapid FRAP rates.

The simulation results show that if the MT dynamic parameters are maintained within a narrow range, then the observed uniform, rapid, and complete FRAP recovery in the preanaphase B spindle can be accounted for even if MT minus ends are restricted to the spindle poles (Fig. 5, A and B; see the supplemental text for details). Specifically, (1) the rescue and catastrophe frequencies should be fast enough ($\sim 0.15 \text{ s}^{-1}$), so the MT growth and shortening cycles are rapid; (2) the growth and shortening rates have to be high enough ($\sim 0.35 \text{ } \mu\text{m/s}$) so that the mean MT length is $\sim 2 \text{ } \mu\text{m}$; and (3) the mean growth length must be slightly smaller than the mean shortening length during the MT growth and shortening cycle (Fig. 5 A).

This model result is further supported by theoretical arguments based on expressing the mean length of MTs, $\langle L \rangle$, in terms of the characteristic lengths, $l_{grow} = v_g/f_{cat}$ and $l_{short} = v_s/f_{res}$, by which the MTs grow and shrink, respectively, within one dynamic instability cycle, and thereby estimating the mean turnover rate (see the supplemental text for details). These arguments suggest that our FRAP observations can be explained if the spindle maintains $f_{res} \sim f_{cat} \sim 0.15 \text{ s}^{-1}$. This predicted order of magnitude is in the same range as previous experimental estimates obtained for metaphase spindles (Rogers et al., 2002; Rusan et al., 2002). Using these arguments, we also predict that the mean length of MTs has to be $\sim 2 \text{ } \mu\text{m}$, whereas $v_g \sim v_s \sim 2 \text{ } \mu\text{m} \times 0.15 \text{ s}^{-1} \sim 0.35 \text{ } \mu\text{m/s}$. Indeed, when we use values within this range in our model, the virtual bleaching of an entire half-spindle (Fig. 5 C and Videos 5 and 6, available at <http://www.jcb.org/cgi/content/full/jcb.200611113/DC1>), of small regions near the spindle pole, or of the equator in preanaphase B spindles, all give rise to FRAP recovery kinetics that account well for our

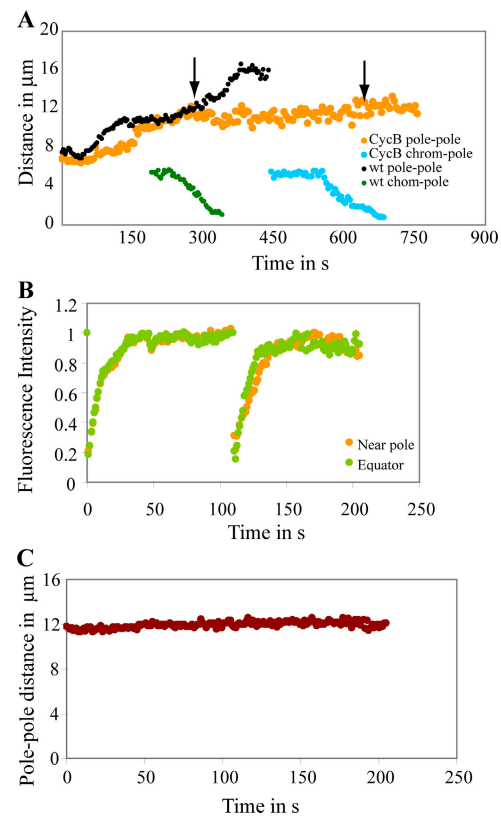
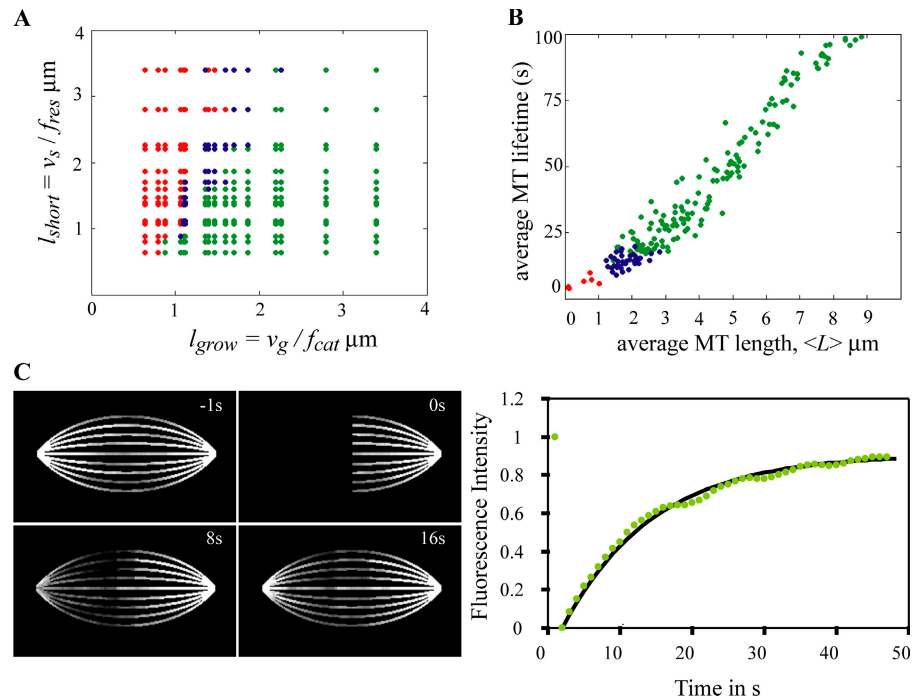


Figure 4. MT turnover and anaphase A after injection of stable GST-cyclin B. (A) Pole-pole and chromosome-to-pole distances in a wild-type (wt) and a stable GST-cyclin B-injected embryo expressing GFP-histone and injected with rhodamine tubulin. In wild type, anaphase B spindle elongation occurs after anaphase A (see arrow), whereas in the spindle with stable GST-cyclin B, no anaphase B occurs (see arrow), even though it undergoes anaphase A, albeit much later and at a slower rate. (B) Fluorescence recovery curves from a FRAP experiment where a spindle in a stable GST-cyclin B-injected embryo was sequentially double bleached near the pole and equator. Both the pole and equatorial regions recover to the same extent during the successive bleaches ($\sim 94\%$ with $t_{1/2}$ of 7.7 and 8 s, and $\sim 96\%$ with $t_{1/2}$ of 6 and 9 s, respectively). Note that the second double bleach was done $>100 \text{ s}$ after the first one, a time scale within which the anaphase B transition happens in a wild-type spindle. (C) Pole-pole distance for the spindle shown in B.

Figure 5. High MT dynamic parameters explain rapid MT turnover in *Drosophila* embryonic spindles. (A and B) Half-times from in silico FRAP of half spindles computed for 256 spindles with varying MT dynamics. The values of MT dynamic parameters used were between 0.1 and 0.3 $\mu\text{m/s}$ for v_g and v_s and 0.05 and 0.25 s^{-1} for f_{cat} and f_{res} in steps of 0.06 $\mu\text{m/s}$ for the velocities and 0.05 s^{-1} for the frequencies. (A) FRAP half-times (colored dots) in terms of the mean growth (l_{grow}) and shrinkage lengths (l_{short}). (B) Same data plotted in terms of the mean length of the MTs, $\langle L \rangle$, and the mean cycle duration ($1/f_{res} + 1/f_{cat}$). Red dots show combinations of MT dynamics where the antiparallel overlap could not be maintained and vanished completely during preanaphase B; blue dots indicate combinations that gave rise to FRAP half-times < 10 s during preanaphase B (rapid and in agreement with our experimental observations); and green dots indicate combinations of parameters that led to FRAP half-times > 10 s (see the supplemental text, available at <http://www.jcb.org/cgi/content/full/jcb.200611113/DC1>). (C, left) Snapshots from a typical in silico FRAP of a half-spindle in preanaphase B. (right) The recovery curve (green dots) and the corresponding exponential fit (black line). $v_g = v_s = 0.34 \mu\text{m/s}$, $f_{res} = 0.2 \text{ s}^{-1}$, and $f_{cat} = 0.25 \text{ s}^{-1}$.



experimental results, that is, a near complete recovery (~ 90 – 95%) and very fast FRAP recovery rate (~ 7 s). Also, under these conditions, the growing MT plus ends are uniformly distributed throughout the preanaphase B spindle (unpublished data).

This result is surprising because, with the minus ends of all MTs anchored to the spindle poles, we had expected the recovery of a bleach region near the spindle pole to be incomplete as a result of the stable portions of the long MTs in the spindle. However, our simulations and theoretical estimates demonstrate that as long as the dynamic instability parameters are adjusted to maintain the mean life cycle of MTs in the order of twice the FRAP half-time, the recovery is uniform, full, and rapid. Therefore, our experimental findings on FRAP and EB1-GFP distribution are entirely consistent with the notion that the *Drosophila* embryo spindles conform to the classic view of centrosome-directed spindle formation pathway with most minus ends anchored to spindle poles. In the alternative case, if MT minus ends are also spatially uniformly distributed in the preanaphase B spindle, the restrictions on the MT dynamic parameters that could account for the observed rapid, full, and uniform FRAP rates relax. However, in this case, the mechanical integrity of the spindle, which then depends on the small and dynamic overlaps between these short interconnected MTs, is compromised (see the supplemental text).

Model result 2: the change in EB1-GFP distribution and the concomitant change in FRAP at anaphase B onset can be accounted for by a spatial gradient in the MT catastrophe frequency

To understand the experimentally observed spatial change in FRAP and in the distribution of growing MT plus ends

(EB1-GFP) at the onset of anaphase B, we considered three different scenarios that could potentially account for the reduced extent of FRAP near the poles at anaphase B: (1) the possibility of a spatial gradient of rescue or catastrophe (Gardner et al., 2005) established at anaphase B onset (Fig. S3 C); (2) a change in the spatial distribution of MT minus ends as a result of the dissociation from the poles of the minus ends of short MTs, which do not overlap with other antiparallel MTs, at anaphase B onset; and (3) an MT-associated protein or motor-dependent differential stabilization of overlapping ipMT plus ends. We found that although the second scenario can, in principle, quantitatively explain the reduced extent of FRAP near the poles during anaphase B, the fit to the data is poor (see the supplemental text). The result of modeling scenario 3 was the induction of an “overgrowth” of overlapping ipMT plus ends into the opposing preanaphase B half-spindles followed by the depletion of growing ipMTs from the equator of anaphase B spindles. Here, the change in ipMT distribution and dynamics was totally inconsistent with the experimental observations (unpublished data). In the context of scenario 1, a rapid establishment of a gradient in rescue frequency at anaphase B onset, with decreased rescue near the poles, explains well the reduced extent of FRAP near the poles but cannot account for the maintenance of numerous growing plus ends at the spindle equator: many MTs that shorten toward the poles vanish, resulting in net loss in both long and short MTs (see the supplemental text). On the other hand, we obtain a very good fit for both the spatial change in FRAP and the distribution of the growing plus ends when we assume that a spatial gradient of catastrophe frequency is established at anaphase B onset, such that the catastrophe frequency increases threefold near the poles (Fig. 6; Fig. S3 C; and Video 7, available at <http://www.jcb.org/cgi/content/full/jcb.200611113/DC1>).

This gradient in catastrophe rate, together with the rapid MT dynamics, leads to an abrupt “sorting” of MTs into short and long ones, thereby rapidly relocating the MT plus ends to the proximity of the poles and to the spindle midzone.

Discussion

Our studies of the dynamic properties of *Drosophila* embryo mitotic spindles using FRAP of GFP-tubulin and time-lapse fluorescence microscopy of EB1-GFP clearly reveal that spindle MTs in this system are extremely dynamic and that there is a reorganization of MTs at the onset of anaphase B; FRAP recovery is decreased near the poles, whereas EB1 is redistributed to the spindle equator. Quantitative modeling suggests that the cell has to fine-tune the MT dynamic instability parameters to achieve the observed rapid MT turnover. Importantly, in the absence of feasible experiments to specifically perturb the critical changes in MT organization and dynamics at anaphase B onset, we used modeling to investigate plausible causes of our observations. This suggests that a spatially nonuniform stabilization of MTs, specifically, a gradient of catastrophe frequencies with a threefold increase at the spindle poles, rapidly evolves at anaphase B onset. The predicted gradient “sorts” the MTs into very short and long ones, giving rise to the MT turnover and plus-end distribution observed experimentally at anaphase B and facilitating spindle elongation (Fig. 7).

What could be the function of the rapid MT turnover during mitosis?

In the *Drosophila* embryo, mitosis takes only 6 min, which is considerably faster than in most other cell types, leading us to speculate that fast MT turnover is an adaptation to fast rates of mitosis. A possible function of rapid turnover could be to relieve elastic MT forces generated by multiple motors, to facilitate the rapid and accurate alignment of the chromosomes at the metaphase plate by eliminating possible long-lasting obstructions, and to ensure the rapid changes in MT length distributions and high motility rates that segregate the chromosomes. The growth and shortening rates and frequencies of catastrophe and rescue predicted by the mathematical model are realistic yet rapid, suggesting that in *Drosophila* embryos, spindle dynamics is as fast as it can be. Modeling also reveals an important yet uncharacterized role for poleward flux in this system: it functions to maintain the integrity of the spindle in face of the rapid MT dynamics, though it contributes minimally to turnover by itself (see the supplemental text).

Our observations raise the question of whether the turnover seen in FRAP during metaphase includes all populations of MTs, including the kinetochore MTs (kMTs). Previous EM studies in mammalian cultured cells indicate that kMTs comprise only a minority of the spindle MTs in metaphase, estimated at ~20% (Brinkley and Cartwright, 1971; McIntosh et al., 1975; Rieder, 1981), and that during metaphase, kMTs display slower dynamics than nonkinetochore MTs (Gorbsky and Borisy, 1989; Zhai et al., 1995). In the absence of relevant EM data, our FRAP experiments do not eliminate the possibility that kMTs form a stable subset, but if so, the rapid and almost complete recovery of

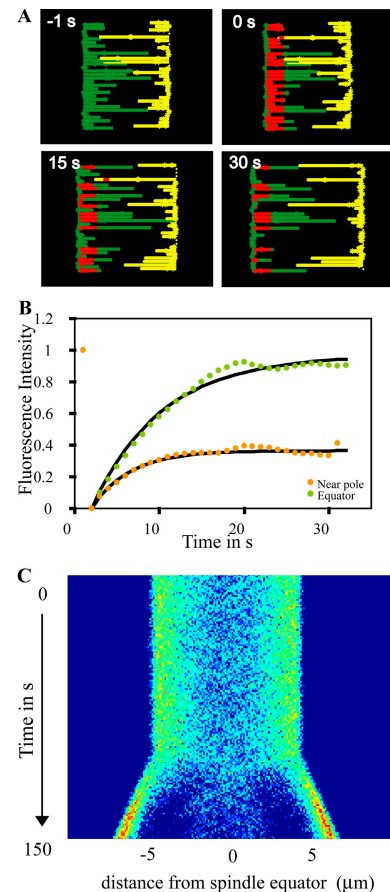


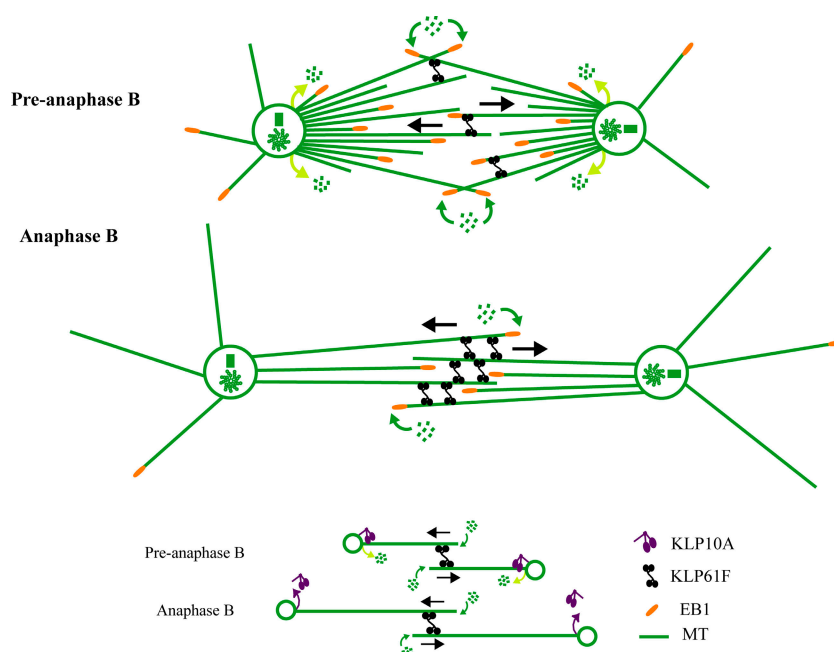
Figure 6. A catastrophe gradient within the spindle at anaphase B onset explains the observed spatial changes in MT dynamics and growing plus-end distribution. (A) Snapshots from in silico FRAP of the pole region of an anaphase B spindle (recovery plot shown in B). See also Video 7 (available at <http://www.jcb.org/cgi/content/full/jcb.200611113/DC1>). The behavior of individual MTs in a single ipMT bundle (30 MTs emanating from opposing poles) is shown. MTs with minus ends anchored to the left and the right pole are shown in green and yellow, respectively. The bleached portions of the MTs after the bleach (0 s) are shown in red. (B) The plot is the normalized fluorescence recovery curves of two in silico bleach zones of an anaphase B spindle with the corresponding exponential fits (black lines); $t_{1/2} = 5.6$ s at the equator and $t_{1/2} = 2.8$ s at the pole. (C) In silico kymograph of the positions of the growing plus ends of MTs over time in a spindle where a catastrophe gradient (with $f_{cat} = 0.15$ s⁻¹ at the equator and three times higher value at the poles; see Fig. S3 C) is introduced at anaphase B onset ($t = 100$ s). The horizontal axis indicates the distance away from the spindle equator. The warmer colors indicate high concentration of growing plus end.

fluorescence, combined with the results of quantitative modeling suggests that the kMTs must comprise only a small proportion of the spindle MTs (see the supplemental text).

Cell cycle-regulated nonuniform stabilization of MTs during anaphase B

In *Drosophila* embryo anaphase B spindles, there is a spatially nonuniform stabilization of MTs along the length of the spindle. This result appears to contrast with yeast and vertebrate systems, where MTs have been shown to be stabilized at anaphase onset (Saxton and McIntosh, 1987; Zhai et al., 1995; Mallavarapu et al., 1999; Maddox et al., 2000; Higuchi and Uhlmann, 2005). It could be that the spatial differences in MT turnover along the

Figure 7. Cartoon showing the reorganization of the plus ends of MTs during preanaphase B and anaphase B. During preanaphase B, there is a uniform distribution of growing MT plus ends as indicated by the presence of EB1 (orange MT tips), whereas MT (green lines) plus ends undergo dynamic instability (green curved arrows). Spindle length is maintained by poleward flux involving ipMT minus-end depolymerization at the poles (light green curved arrows) coupled to outward sliding by the bipolar kinesin-5, KLP61F (solid black arrows). At anaphase B onset, a catastrophe gradient abruptly evolves, leading to a swift change in the MT lengths and thereby rapidly relocalizing the growing ipMT plus ends to the spindle midzone. The sustained presence of growing ipMT plus ends at the equator during anaphase B serves to maintain robust anti-parallel ipMT bundles on which KLP61F generates the forces that push the poles apart. (bottom) A simplified version of our model for anaphase B (Brust-Mascher et al., 2004) where, in preanaphase B spindles, depolymerization by KLP10A at the poles balances the sliding of ipMTs by KLP61F, but depolymerization at the poles ceases at anaphase B onset, allowing persistent ipMT sliding to drive pole–pole separation.



spindle were missed in previous experiments in vertebrates. It is also possible that *Drosophila* and higher organisms behave differently from *Saccharomyces cerevisiae* or *Schizosaccharomyces pombe*, two systems where changes in MT dynamics have been measured carefully during different stages of mitosis (Mallavarapu et al., 1999; Higuchi and Uhlmann, 2005).

Our data obtained using a nondegradable cyclin B construct suggests that spindles must progress through metaphase and anaphase A before the changes in MT dynamics and plus-end distribution characteristic of anaphase B onset can occur. This indicates that these dynamic changes are not an intrinsic property of the spindle MTs themselves, resulting, for example, from MT lifetime–related posttranslational modifications, but are cell cycle regulated instead. In addition, our results also suggest that chromosome segregation is not sufficient to trigger anaphase B, in agreement with previous studies showing that cyclin B degradation was required to exit anaphase A in *Drosophila* embryos (Su et al., 1998; Parry and O'Farrell, 2001).

Molecular mechanism of the spatial change in MT dynamics at anaphase B onset

An important question relates to the nature of events downstream of cyclin B degradation that lead to the observed spatial changes in MT dynamics and distribution. Experiments aimed at targeting specific proteins or mechanisms, such as a Ran-regulated MT stabilization or the requirement of tight bundling of ipMTs by the kinesin KLP3A, did not provide conclusive experimental evidence. Spindles that exhibited some level of anaphase B spindle elongation always displayed EB1 redistribution, but it was not possible to quantitatively correlate the level of elongation with the extent of MT plus-end redistribution. In addition, the proteins that are likely to contribute to this reorganization also have other roles in mitosis. For example, the kinesin-13 depolymerases, KLP10A, KLP59C, and KLP59D, might play a role in the establishment of a catastrophe gradient

at anaphase B (Mennella et al., 2005). Of these, KLP10A at the spindle poles is in an appropriate position to increase the catastrophe frequency at the poles of the anaphase B spindle, but its inhibition causes several mitotic defects before anaphase B, obscuring its specific role at this stage (Rogers et al., 2004).

It is possible that systematic genetic screens or the evaluation of other plausible candidates, like the *Drosophila* homologue of PRC-1 (Verni et al., 2004; Zhu et al., 2006), will reveal the identity of the molecules involved, but this lies outside the scope of the current study. This could be challenging because the relevant regulatory mechanism may be complex, involving multiple molecular players and perhaps other mechanical factors (at the end of this section) that lead to the establishment of the catastrophe gradient and the maintenance of the high dynamic instability rates predicted by our model.

An alternative mechanistic explanation for the establishment of the catastrophe gradient is based on the well-established idea that forces such as tension or compression are able to regulate the dynamics of MT ends, either through direct mechanical effects or through the regulation of molecules that are able to alter MT dynamics. For example, it is proposed that high tension at the kinetochore inactivates the kinesin-13 at the kMT plus ends (Gardner et al., 2005). Again, experimental tests of this or similar hypotheses lie outside the scope of the current study.

Model for the anaphase B switch

We conclude that in *Drosophila* embryo mitosis, the spindle undergoes an abrupt, spatial change in MT dynamics at anaphase B onset that accompanies the abrupt suppression of depolymerization at the poles reported previously (Fig. 7; Brust-Mascher and Scholey, 2002; Brust-Mascher et al., 2004). Furthermore, this anaphase A–anaphase B transition is regulated by cyclin B degradation (and presumably Cdk inactivation). Before this switch, the preanaphase B ipMTs are slid apart by a kinesin-5–driven sliding filament mechanism and are depolymerized by

kinesin-13 at the spindle poles to generate a force balance that maintains an isometric, steady-state spindle length and also generates poleward flux within ipMTs (Fig. 7, bottom). Although poleward flux contributes to chromatid-to-pole motion and constrains preanaphase B spindle length (Brust-Mascher et al., 2004), the maintenance of high dynamics at MT plus ends throughout the spindle may contribute to the rapid and accurate positioning of sister chromatids at the metaphase plate. At the onset of anaphase B, when the sister chromatids have reached the spindle poles, the establishment of a catastrophe gradient effectively separates MTs into two groups: long ones extending from the pole to the spindle equator that are slid apart to drive the elongation of the spindle, and short ones with plus ends close to the poles that may contribute to the maintenance of the chromatids at the poles. Thus, at this stage, MTs that are not directly involved in force generation depolymerize and disappear, yielding free subunits capable of adding on to the subset of overlapping ipMTs, on which the bipolar motors generate the force for anaphase spindle elongation. The maintenance of the high levels of net ipMT polymerization ensures the sustained and steady sliding of ipMTs by kinesin-5 motors for a robust and complete spindle elongation (see Fig. 4 E in Brust-Mascher et al., 2004). As a result of this transition, the elongating anaphase B spindle acquires a more organized and compact structure, which facilitates pole–pole separation.

Thus, our model suggests that the anaphase B switch uses a form of biased “search and capture” analogous to that involved in prometaphase chromosome capture. We propose that dynamically unstable MTs “search” the preanaphase B spindle, but the establishment of the predicted catastrophe gradient at anaphase B onset biases this search, increasing the tendency of ipMTs from one pole to “capture” ipMTs from the other pole, thereby augmenting the equatorial ipMT overlap zone, where the force for spindle elongation is generated.

Materials and methods

Drosophila stocks and embryo preparation

Flies were maintained at 25°C, and 0–2-h embryos were collected as described previously (Ashburner, 1989). Flies expressing GFP-tubulin were provided by A. Spradling (Carnegie Institution, Washington, DC) and those expressing GFP-histone by B. Sullivan (University of California, Santa Cruz, Santa Cruz, CA). The EB1-GFP transgenic fly was a gift from S. Rogers (University of North Carolina at Chapel Hill, Chapel Hill, NC), B. Eaton, and G. Davis (University of California, San Francisco, San Francisco, CA). The EB1-GFP transgene, a C-terminal GFP fusion to EB1 (pUASp-EB1-GFP) was expressed under the UASp promoter. Germ line expression of pUASp-GFP-EB1 transgene was driven by using the tubulin Gal4 drivers *tub* ([*matα4*]GAL4-VP16-V2H) or *tub* ([*matα4*]GAL4-VP16-V37).

Purification of GST-cyclin B

GST-cyclin B (provided by D. Kellogg, University of California, Santa Cruz, Santa Cruz, CA) was purified from *Escherichia coli* as described previously (Kellogg et al., 1995). During the final elution step, the protein was eluted using 10 mM glutathione in 50 mM Tris, pH 8.1, and 0.3 M KCl. The eluted protein was dialyzed into 50 mM Hepes, pH 7.6, 0.125 M KCl, and 10% glycerol and concentrated to 10 mg/ml for injection into embryos.

Microscopy and image analysis

FRAP experiments were done on a laser-scanning confocal microscope (FV1000; Olympus) with a 60× 1.40 NA objective at 23°C, and image acquisition was done using the Fluoview software (version 1.5; Olympus). The embryos expressing GFP-tubulin were dechorionated and kept in halo-

carbon oil to prevent dehydration and were imaged using the 488-nm line from an argon laser. A separate 405-nm laser was used to photobleach GFP-tubulin. The use of two different lasers allowed simultaneous imaging and bleaching. The spindle was bleached in rectangular or circular areas of defined width and diameter, respectively, and images were acquired every 1.1 s. The spindles were corrected for movement using MatLab (Mathworks), and the fluorescence intensities within the bleached region were measured using MetaMorph imaging software (Universal Imaging Corp.). The fluorescence intensity of the bleached region over time was normalized with the prebleached fluorescence intensity and was plotted as a function of time. The recovery half-time was obtained by fitting a single exponential curve $= F_0 + (F_{inf} - F_0) (1 - e^{-t})$ (Salmon et al., 1984) to the recovery time course curve. The images were not corrected for bleaching because it was not feasible to find an unbleached spot devoid of MT alterations within the embryos during anaphase B. Time-lapse microscopy of EB1-GFP-, GFP-tubulin-, and GFP-histone-expressing embryos was done on a microscope (Olympus) equipped with an UltraView spinning disk confocal head (PerkinElmer) with a 100× 1.35 NA objective. The embryos were prepared as outlined in the beginning of this section and kept in halocarbon oil. Images were acquired using the UltraView software (PerkinElmer) at a rate of 1.5 s/frame at 23°C and recorded using a digital camera (ORCA ER; Hamamatsu). Embryos expressing EB1-GFP and GFP-histone were injected with rhodamine tubulin (Cytoskeleton) to visualize MTs. Images were analyzed using MetaMorph. The images were processed using the “No Neighbors” Deconvolution and Low Pass Filter commands. The whole spindle kymograph was done using MatLab.

Online supplemental material

Fig. S1 shows a metaphase spindle bleached at the equator and FRAP of a spindle in the presence of taxol. Fig. S2 shows a plot of spindle pole distance versus time in the presence of GST-cyclin B, kymographs of tubulin and EB1 intensity in the wild-type and GST-cyclin B-injected embryo, and EB1 distribution in the presence of anti-KLP3A antibody and RanT24N. Fig. S3 provides illustrations of possible organization of MT minus ends in the spindle and shows the predicted spatial gradients of MT dynamic parameters in the spindle, as well as a kymograph of tubulin and EB1 intensity from prometaphase through anaphase B and a kymograph of the positions of growing MT plus ends in a virtual spindle from prometaphase through anaphase B. Video 1 shows FRAP of a metaphase spindle, and Videos 2 and 3 show the simultaneous double bleaching of pole and equator of a metaphase and anaphase B spindle, respectively. Video 4 shows the time lapse of an EB1-GFP-expressing embryo injected with rhodamine tubulin. Video 5 shows a typical in silico FRAP of a virtual spindle in preanaphase B. Video 6 shows the fluorescence recovery of individual MTs in an ipMT bundle of the spindle in Video 5. Video 7 shows the fluorescence recovery of individual MTs in an ipMT bundle of a virtual spindle in anaphase B, before and after in silico bleaching. Video 8 shows the fluorescence recovery of individual MTs in an ipMT bundle of a virtual spindle in preanaphase B without poleward flux, before and after in silico bleaching.

We thank Roy Wollman for the great help with image analysis, Dr. Doug Kellogg for the stable GST-cyclin B plasmid, Dr. Andrew Wilde for Ran reagents, Dr. Steve Rogers for GFP-EB1 stocks, Dr. Frank McNally for critical reading of the manuscript, and the cytoskeleton group at the University of California at Davis and other members of the Scholey laboratory for discussion.

This work was supported by National Institutes of Health grants GM068952 to A. Mogilner and J.M. Scholey and GM55507 to J.M. Scholey.

Submitted: 20 November 2006

Accepted: 15 May 2007

References

- Ashburner, M. 1989. *Drosophila: A Laboratory Handbook*. Cold Spring Harbor Laboratory Press. Cold Spring Harbor, NY. 1331 pp.
- Brinkley, B.R., and J. Cartwright Jr. 1971. Ultrastructural analysis of mitotic spindle elongation in mammalian cells in vitro: direct microtubule counts. *J. Cell Biol.* 50:416–431.
- Brust-Mascher, I., and J.M. Scholey. 2002. Microtubule flux and sliding in mitotic spindles of *Drosophila* embryos. *Mol. Biol. Cell.* 13:3967–3975.
- Brust-Mascher, I., G. Civelekoglu-Scholey, M. Kwon, A. Mogilner, and J.M. Scholey. 2004. Model for anaphase B: role of three mitotic motors in a switch from poleward flux to spindle elongation. *Proc. Natl. Acad. Sci. USA.* 101:15938–15943.

- Burbank, K.S., A.C. Groen, Z.E. Perlman, D.S. Fisher, and T.J. Mitchison. 2006. A new method reveals microtubule minus ends throughout the meiotic spindle. *J. Cell Biol.* 175:369–375.
- Civelekoglu-Scholey, G., D.J. Sharp, A. Mogilner, and J.M. Scholey. 2006. Model of chromosome motility in *Drosophila* embryos: adaptation of a general mechanism for rapid mitosis. *Biophys. J.* 90:3966–3982.
- Gadde, S., and R. Heald. 2004. Mechanisms and molecules of the mitotic spindle. *Curr. Biol.* 14:R797–R805.
- Gardner, M.K., C.G. Pearson, B.L. Sprague, T.R. Zarzar, K. Bloom, E.D. Salmon, and D.J. Odde. 2005. Tension-dependent regulation of microtubule dynamics at kinetochores can explain metaphase congression in yeast. *Mol. Biol. Cell.* 16:3764–3775.
- Gorbsky, G.J., and G.G. Borisy. 1989. Microtubules of the kinetochore fiber turn over in metaphase but not in anaphase. *J. Cell Biol.* 109:653–662.
- Higuchi, T., and F. Uhlmann. 2005. Stabilization of microtubule dynamics at anaphase onset promotes chromosome segregation. *Nature.* 433:171–176.
- Kalab, P., A. Pralle, E.Y. Isacoff, R. Heald, and K. Weis. 2006. Analysis of a RanGTP-regulated gradient in mitotic somatic cells. *Nature.* 440:697–701.
- Kellogg, D.R., A. Kikuchi, T. Fujii-Nakata, C.W. Turck, and A.W. Murray. 1995. Members of the NAP/SET family of proteins interact specifically with B-type cyclins. *J. Cell Biol.* 130:661–673.
- Kwon, M., S. Morales-Mulia, I. Brust-Mascher, G.C. Rogers, D.J. Sharp, and J.M. Scholey. 2004. The chromokinesin, KLP3A, drives mitotic spindle pole separation during prometaphase and anaphase and facilitates chromatid motility. *Mol. Biol. Cell.* 15:219–233.
- Maddox, P.S., K.S. Bloom, and E.D. Salmon. 2000. The polarity and dynamics of microtubule assembly in the budding yeast *Saccharomyces cerevisiae*. *Nat. Cell Biol.* 2:36–41.
- Mahoney, N.M., G. Goshima, A.D. Douglass, and R.D. Vale. 2006. Making microtubules and mitotic spindles in cells without functional centrosomes. *Curr. Biol.* 16:564–569.
- Mallavarapu, A., K. Sawin, and T. Mitchison. 1999. A switch in microtubule dynamics at the onset of anaphase B in the mitotic spindle of *Schizosaccharomyces pombe*. *Curr. Biol.* 9:1423–1426.
- McIntosh, J.R., W.Z. Cande, and J.A. Snyder. 1975. Structure and physiology of the mammalian mitotic spindle. *Soc. Gen. Physiol. Ser.* 30:31–76.
- McIntosh, J.R., K.L. McDonald, M.K. Edwards, and B.M. Ross. 1979. Three-dimensional structure of the central mitotic spindle of *Diatoma vulgare*. *J. Cell Biol.* 83:428–442.
- Mennella, V., G.C. Rogers, S.L. Rogers, D.W. Buster, R.D. Vale, and D.J. Sharp. 2005. Functionally distinct kinesin-13 family members cooperate to regulate microtubule dynamics during interphase. *Nat. Cell Biol.* 7:235–245.
- Mitchison, T., and M. Kirschner. 1984. Dynamic instability of microtubule growth. *Nature.* 312:237–242.
- Mitchison, T.J., and E.D. Salmon. 1992. Poleward kinetochore fiber movement occurs during both metaphase and anaphase-A in newt lung cell mitosis. *J. Cell Biol.* 119:569–582.
- Parry, D.H., and P.H. O'Farrell. 2001. The schedule of destruction of three mitotic cyclins can dictate the timing of events during exit from mitosis. *Curr. Biol.* 11:671–683.
- Piehl, M., and L. Cassimeris. 2003. Organization and dynamics of growing microtubule plus ends during early mitosis. *Mol. Biol. Cell.* 14:916–925.
- Pines, J. 2006. Mitosis: a matter of getting rid of the right protein at the right time. *Trends Cell Biol.* 16:55–63.
- Rieder, C.L. 1981. The structure of the cold-stable kinetochore fiber in metaphase PtK1 cells. *Chromosoma.* 84:145–158.
- Rogers, G.C., S.L. Rogers, T.A. Schwimmer, S.C. Ems-McClung, C.E. Walczak, R.D. Vale, J.M. Scholey, and D.J. Sharp. 2004. Two mitotic kinesins cooperate to drive sister chromatid separation during anaphase. *Nature.* 427:364–370.
- Rogers, S.L., G.C. Rogers, D.J. Sharp, and R.D. Vale. 2002. *Drosophila* EB1 is important for proper assembly, dynamics, and positioning of the mitotic spindle. *J. Cell Biol.* 158:873–884.
- Royou, A., W. Sullivan, and R. Karess. 2002. Cortical recruitment of nonmuscle myosin II in early syncytial *Drosophila* embryos: its role in nuclear axial expansion and its regulation by Cdc2 activity. *J. Cell Biol.* 158:127–137.
- Rusan, N.M., U.S. Tulu, C. Fagerstrom, and P. Wadsworth. 2002. Reorganization of the microtubule array in prophase/prometaphase requires cytoplasmic dynein-dependent microtubule transport. *J. Cell Biol.* 158:997–1003.
- Salmon, E.D., R.J. Leslie, W.M. Saxton, M.L. Karow, and J.R. McIntosh. 1984. Spindle microtubule dynamics in sea urchin embryos: analysis using a fluorescein-labeled tubulin and measurements of fluorescence redistribution after laser photobleaching. *J. Cell Biol.* 99:2165–2174.
- Saxton, W.M., and J.R. McIntosh. 1987. Interzone microtubule behavior in late anaphase and telophase spindles. *J. Cell Biol.* 105:875–886.
- Saxton, W.M., D.L. Stemple, R.J. Leslie, E.D. Salmon, M. Zavortink, and J.R. McIntosh. 1984. Tubulin dynamics in cultured mammalian cells. *J. Cell Biol.* 99:2175–2186.
- Scholey, J.M., I. Brust-Mascher, and A. Mogilner. 2003. Cell division. *Nature.* 422:746–752.
- Sharp, D.J., K.L. McDonald, H.M. Brown, H.J. Matthies, C. Walczak, R.D. Vale, T.J. Mitchison, and J.M. Scholey. 1999. The bipolar kinesin, KLP61F, cross-links microtubules within interpolar microtubule bundles of *Drosophila* embryonic mitotic spindles. *J. Cell Biol.* 144:125–138.
- Silverman-Gavrila, R.V., and A. Wilde. 2006. Ran is required before metaphase for spindle assembly and chromosome alignment and after metaphase for chromosome segregation and spindle midbody organization. *Mol. Biol. Cell.* 17:2069–2080.
- Su, T.T., F. Sprenger, P.J. DiGregorio, S.D. Campbell, and P.H. O'Farrell. 1998. Exit from mitosis in *Drosophila* syncytial embryos requires proteolysis and cyclin degradation, and is associated with localized dephosphorylation. *Genes Dev.* 12:1495–1503.
- Verni, F., M.P. Somma, K.C. Gunsalus, S. Bonaccorsi, G. Belloni, M.L. Goldberg, and M. Gatti. 2004. Feo, the *Drosophila* homolog of PRC1, is required for central-spindle formation and cytokinesis. *Curr. Biol.* 14:1569–1575.
- Wadsworth, P., and E.D. Salmon. 1986. Analysis of the treadmilling model during metaphase of mitosis using fluorescence redistribution after photobleaching. *J. Cell Biol.* 102:1032–1038.
- Wadsworth, P., and A. Khodjakov. 2004. E pluribus unum: towards a universal mechanism for spindle assembly. *Trends Cell Biol.* 14:413–419.
- Wheatley, S.P., E.H. Hinchcliffe, M. Glotzer, A.A. Hyman, G. Sluder, and Y. Wang. 1997. CDK1 inactivation regulates anaphase spindle dynamics and cytokinesis in vivo. *J. Cell Biol.* 138:385–393.
- Wollman, R., E.N. Cytrynbaum, J.T. Jones, T. Meyer, J.M. Scholey, and A. Mogilner. 2005. Efficient chromosome capture requires a bias in the 'search-and-capture' process during mitotic-spindle assembly. *Curr. Biol.* 15:828–832.
- Zhai, Y., P.J. Kronebusch, and G.G. Borisy. 1995. Kinetochore microtubule dynamics and the metaphase-anaphase transition. *J. Cell Biol.* 131:721–734.
- Zhu, C., E. Lau, R. Schwarzenbacher, E. Bossy-Wetzel, and W. Jiang. 2006. Spatiotemporal control of spindle midzone formation by PRC1 in human cells. *Proc. Natl. Acad. Sci. USA.* 103:6196–6201.